p37/UBXN2B regulates spindle orientation by limiting cortical NuMA recruitment via PP1/Repo-Man

Byung Ho Lee,[1] Francoise Schwager,[1,2] Patrick Meraldi,[1] and Monica Gotta[1,2]

[1]Department of Cell Physiology and Metabolism and [2]Swiss National Centre for Competence in Research in Chemical Biology, University of Geneva, Geneva, Switzerland

Spindle orientation determines the axis of division and is crucial for cell fate, tissue morphogenesis, and the development of an organism. In animal cells, spindle orientation is regulated by the conserved Gαi–LGN–NuMA complex, which targets the force generator dynein–dynactin to the cortex. In this study, we show that p37/UBXN2B, a cofactor of the p97 AAA ATPase, regulates spindle orientation in mammalian cells by limiting the levels of cortical NuMA. p37 controls cortical NuMA levels via the phosphatase PP1 and its regulatory subunit Repo-Man, but it acts independently of Gαi, the kinase Aurora A, and the phosphatase PP2A. Our data show that in anaphase, when the spindle elongates, PP1/Repo-Man promotes the accumulation of NuMA at the cortex. In metaphase, p37 negatively regulates this function of PP1, resulting in lower cortical NuMA levels and correct spindle orientation.

JOURNAL OF CELL BIOLOGY

Introduction

Mitotic spindle orientation determines the axis of cell division and plays a key role in cell fate determination in tissues (Panousopoulou and Green, 2014). Spindle orientation is controlled by forces exerted by cortical dynein–dynactin motor complexes on the astral microtubules emanating from the spindle poles (di Pietro et al., 2016). The strength of these forces is proportional to the abundance of motor complexes at the cortex (Du and Macara, 2004; Kotak et al., 2012). In metaphase, dynein–dynactin is recruited via the conserved Gαi–leucine-glycine-asparagine (LGN)–nuclear and mitotic apparatus (NuMA) complex: Gαi, a G protein α subunit, anchors the complex at the plasma membrane, LGN bridges the GDP-bound form of Gαi and the C terminus of NuMA, and NuMA recruits the dynein–dynactin complex to the cortex via its N terminus (di Pietro et al., 2016). The NuMA–dynein–dynactin complex is also present at spindle poles, where it physically tethers kinetochore fibers to focus the poles (Merdes et al., 1996; Gordon et al., 2001). In anaphase, additional Gαi/LGN-independent platforms recruit NuMA to the cortex, including the actin-binding protein 4.1R/G and phosphoinositides (Kiyomitsu and Cheeseman, 2013; Seldin et al., 2013; Kotak et al., 2014; Zheng et al., 2014).

NuMA recruitment to the cortex must be tightly controlled, as both too little and too much cortical NuMA impairs spindle orientation (Du and Macara, 2004; Kotak et al., 2012). In metaphase, NuMA phosphorylation by Cdk1 displaces it from the cortex, directing it to spindle poles. When CDK1 activity drops at anaphase onset, the protein phosphatase PP2A dephosphorylates NuMA, resulting in cortical enrichment (Kotak et al., 2013; Zheng et al., 2014). Conversely, Aurora A phosphorylation directs NuMA to the cortex (Gallini et al., 2016; Kotak et al., 2016). Finally, the Plk1 kinase displaces LGN and dynein–dynactin when centrosomes or unaligned chromosomes come too close to the cortex (Kiyomitsu and Cheeseman, 2012; Tame et al., 2016). This regulation ensures appropriate levels of cortical dynein to orient the spindle in metaphase and to elongate it in anaphase.

Our recent work identified p37, a cofactor of the $p97^{CDC48}$ AAA ATPase, as a regulator of spindle orientation (Kress et al., 2013). $p97^{CDC48}$ regulates multiple processes both in interphase and mitosis. It hydrolyzes ATP to segregate modified substrates from cellular structures, multiprotein complexes, and chromatin, and targets them either to degradation or recycling (Yamanaka et al., 2012). Functional specificity is given by p97 adapters such as p37. How p37 controls spindle orientation is, however, unknown. In this study, we find that p37 ensures proper spindle orientation by preventing the excessive recruitment of NuMA to the cortex in metaphase. Epistasis experiments indicate that p37 acts in a Gαi/LGN-independent manner via the protein phosphatase PP1 and its regulatory subunit Repo-Man, which promote NuMA recruitment to the cortex.

Results and discussion

p37 regulates spindle orientation by limiting cortical NuMA levels

In tissue culture cells with an intact spindle orientation control, the mitotic spindle is oriented parallel to the growth surface, whereas spindle orientation defects result in a higher median angle between the spindle and the growth surface (called from here on "spindle angle"; Figs. 1 A and S1 A; Toyoshima and Nishida, 2007). As we previously showed, p37 depletion in

Correspondence to Patrick Meraldi: patrick.meraldi@unige.ch; Monica Gotta: monica.gotta@unige.ch

The Rockefeller University Press
J. Cell Biol. Vol. 217 No. 2 483–493
https://doi.org/10.1083/jcb.201707050

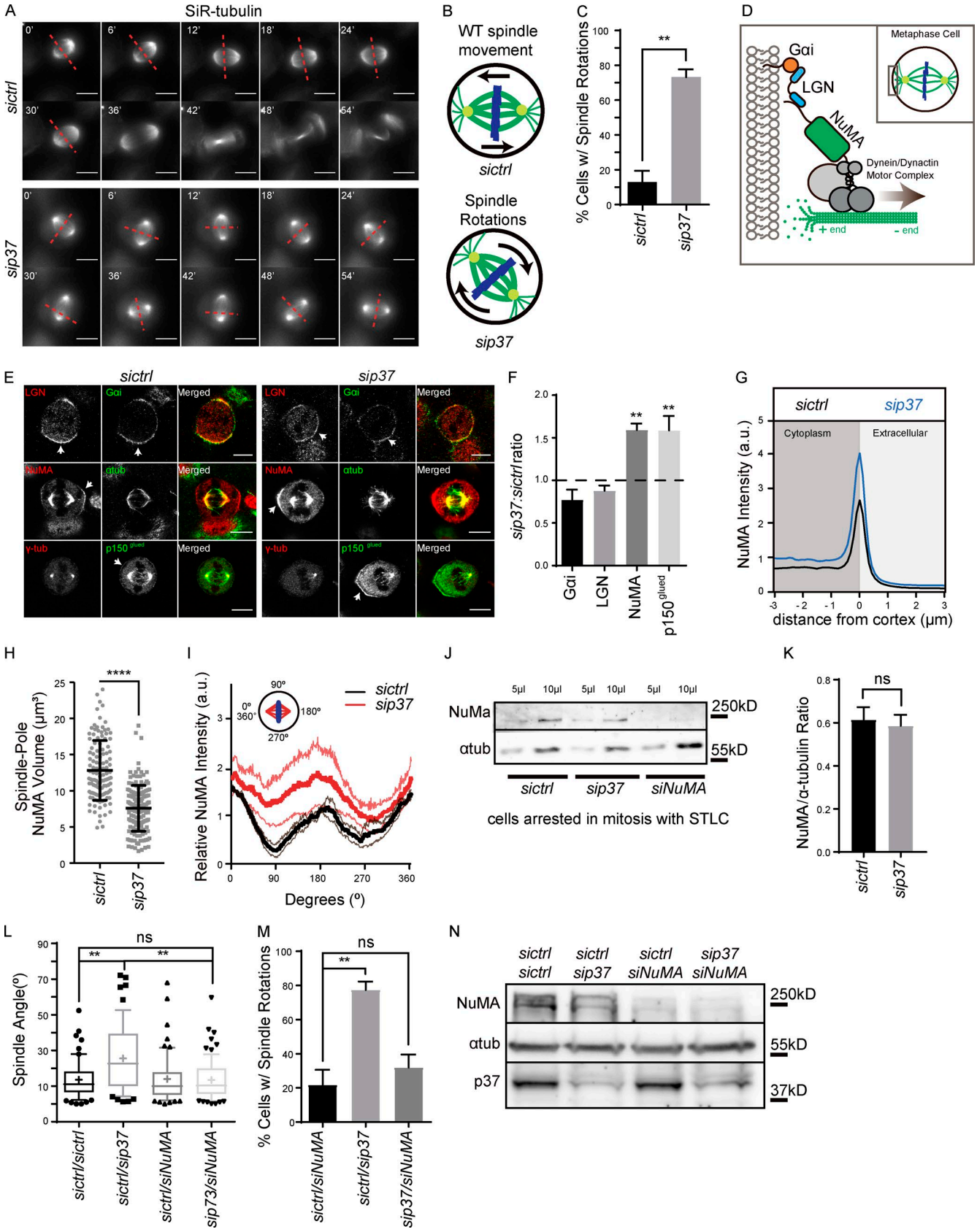

Figure 1. **p37 regulates spindle orientation by limiting cortical NuMA levels. (A)** Time-lapse images of *siControl* and *sip37* HeLa cells stained with SiR-tubulin (live microtubule marker). Red dashed lines indicate the metaphase plate position. Unless otherwise stated, analyses were performed on metaphase cells throughout the paper. *t* = 0 was set at the first image with a bipolar spindle. **(B)** Schematics of cells with WT spindle movements (top) and excessive spindle rotations (bottom). Black arrows indicate spindle movements. **(C)** Mean percentages of cells with excessive spindle rotations (when on average the

HeLa cells increased the spindle angle when compared with control treatment (Fig. S1, A–D; Kress et al., 2013). This effect is rescued by exogenous p37 expression, indicating that this is not a result of an off-target effect (Kress et al., 2013). To understand how p37 controls spindle orientation, we depleted it in HeLa cells, labeled the spindle with SiR-tubulin, a live microtubule marker (Lukinavičius et al., 2014), and monitored it by time-lapse imaging. In *siControl* cells, the mitotic spindle remained parallel to the growth substratum and oscillated along the spindle axis (Fig. 1, A–C). In contrast, in 73% of *sip37* cells, the mitotic spindle exhibited excessive oscillations in all axes, with a mean spindle rotation of 20.5° every 3 min (called spindle rotations from now on; Fig. 1, A–C; and Fig. S1 B), confirming our previous study (Kress et al., 2013). These orientation defects appeared immediately after mitotic entry, implying that they were not caused by a prolonged mitotic arrest, in contrast with other protein depletions that only deregulate spindle orientation several hours into a mitotic arrest (Tame et al., 2016).

These excessive spindle rotations were similar to the ones observed in cells overexpressing Gαi, LGN, or NuMA (Fig. 1 D; Du and Macara, 2004; Kotak et al., 2012). We therefore immunostained *siControl* and *sip37* cells against Gαi, LGN, NuMA, and p150^{glued} (a dynein–dynactin subunit) and quantified their levels at the cortex. Both p150^{glued} and NuMA levels were increased by 50% in *sip37* cells, whereas Gαi and LGN levels were unchanged (Fig. 1, E and F). NuMA has a complex localization pattern, as it forms large crescents at spindle poles and is present in the cytoplasm and the cortex (Fig. 1 E). At the cortex, NuMA is enriched proximal to spindle poles and is displaced from regions close to the chromatin via the Ran-GTP gradient (Fig. 1 E; Kiyomitsu and Cheeseman, 2012; Bird et al., 2013). We used line profiles in *siControl* and *sip37* cells to quantify cortical and cytoplasmic NuMA levels and a threshold function to measure the volume it occupies at spindle poles (Fig. S3, D–F). p37 depletion increased cortical NuMA levels by 48% and in the cytoplasm by 22% (Fig. 1 G) but decreased the volume of NuMA spindle pole crescents by 41% (Fig. 1 H). The increase in cortical levels did not reflect a disruption of local regulation, as NuMA was still enriched proximal to the spindle poles (Fig. 1 I). Immunoblotting of *siControl* and *sip37* cell extracts revealed constant total cellular NuMA levels (Fig. 1, J and K), indicating that p37 specifically regulates NuMA localization. The increase in cortical NuMA levels was responsible for the spindle orientation defects, as partial NuMA codepletion restored normal spindle angles (Fig. 1 L) and suppressed the excessive spindle rotations (Fig. 1 M) in *sip37* cells; it did not, however, change the spindle angle in *siControl* cells. This rescue was not caused by an RNAi competition effect because p37 was depleted to the same extent whether NuMA was codepleted or not (Fig. 1 N). We conclude that p37 controls spindle orientation by limiting the amount of cortical NuMA in metaphase.

High cortical NuMA levels in *sip37* cells depend on a protein phosphatase activity

p37 depletion did not affect cortical Gαi and LGN levels, but it increased cortical NuMA levels, suggesting a Gαi-independent recruitment. To test this hypothesis, we codepleted Gαi and p37. Gαi depletion abolished cortical NuMA in control metaphase cells as previously shown (Fig. 2, A–C; Woodard et al., 2010), but it left a cortical NuMA pool in *sip37* cells (Fig. 2, A and B). Equivalent results were observed after LGN depletion (Fig. S1, E–H), implying that a pool of cortical NuMA in *sip37* cells is recruited in a Gαi/LGN-independent manner.

Aurora A phosphorylates NuMA in metaphase to promote its cortical enrichment (Fig. 2 D; Gallini et al., 2016; Kotak et al., 2016). Because p37 depletion increases the centrosomal levels of Aurora A in prophase (Kress et al., 2013), we tested whether the increase in cortical NuMA levels depended on Aurora A. We inhibited Aurora A activity in *siControl* and *sip37* cells using 20 nM MLN8237 for 24 h and then quantified cortical NuMA levels. This treatment impaired Aurora A activity, as assessed by phospho-T288 antibodies recognizing active Aurora A, and severely reduced cortical NuMA levels (Fig. 2, E–H). Nonetheless, p37 depletion still increased cortical NuMA in MLN8237-treated cells, indicating that p37 can regulate NuMA independently of Aurora A (Fig. 2, G and H).

Phosphorylation by Cdk1 negatively regulates NuMA cortical localization, whereas dephosphorylation by PP2A promotes it (Fig. 2 D; Kotak et al., 2013; Zheng et al., 2014). High cortical levels of NuMA in *sip37* are unlikely to be a result of low Cdk1 activity because *sip37* cells enter mitosis with no significant delay (unpublished data) and show no changes in the levels of epitopes stained by MPM2, a phosphoantibody that recognizes Cdk1 phosphorylation targets (Fig. S1, I and J; Westendorf et al., 1994). To test the involvement of a phosphatase, we treated *sip37* cells with the phosphatase inhibitor calyculin A (50 nM for 10 min). As previously shown, this treatment prevented cortical NuMA recruitment in *siControl* cells (Kotak et al., 2013). It also abolished the increase in cortical NuMA levels seen after p37 siRNA (Fig. 2, I and J) but did not alter the cortical Gαi and LGN levels (Fig. S1, K and L). We conclude that p37 limits cortical NuMA levels by preventing the action of a phosphatase.

spindle rotates >10° per 3-min time point). *n* = 3 independent experiments; *n* = 83–96 cells. **, P = 0.0077 in a paired *t* test. **(D)** Schematics representing the ternary complex that generates forces on microtubules. **(E)** Confocal images of *siControl* and *sip37* cells immunostained for α-tubulin (microtubules), γ-tubulin (spindle poles), Gαi, LGN, NuMA, or p150^{glued}, as indicated. White arrows point to the cortical localization of these proteins. **(F)** Quantification of mean cortical intensities of Gαi, LGN, NuMA, and p150^{glued} in p37-depleted cells normalized to *siControl* (dashed line). *n* = 4–5; *n* = 74–140 cells. P < 0.0001 in a one-way ANOVA test; **, P < 0.01 versus control. **(G)** Quantification of cytoplasmic and cortical NuMA levels in *siControl* and *sip37* cells. The quantification is shown as a line profile representing the mean intensity across the cortex. *n* = 4; *n* = 86–87. The cortex is at the border between the cytoplasm (dark gray) and the extracellular environment (light gray). **(H)** Quantification of spindle pole NuMA volume in cells with the indicated depletions. *n* = 3; spindle poles = 120–159. ****, P < 0.0001 in an unpaired *t* test. **(I)** Mean intensity profile of cortical NuMA along the entire cortex relative to the spindle (x and y axis) in *siControl* (black) and *sip37* cells (red). *n* = 3; *n* = 79–85. **(J)** Western blot of mitotic cell lysates treated with indicated siRNAs and probed against NuMA and α-tubulin (loading control). **(K)** Quantification of NuMA/α-tubulin ratio signal in three Western blots as shown in J in *siControl* and *sip37* cell extracts. **(L)** Quantification of spindle angles in *siControl* and *sip37* fixed cells stained against γ-tubulin as shown in Fig. S3 A. Data are shown as box plots. Each point represents a cell; + indicates the mean spindle angle. *n* = 4; *n* = 57–75 cells. **, P < 0.01 in a Kruskal-Wallis test. **(M)** Mean percentages of HeLa–dynein heavy chain–GFP cells with spindle rotations after indicated siRNAs. *n* = 3; *n* = 50–59 cells. Error bars indicate SEM (C, F, I, K, and M) or SD (H). **, P = 0.0093 in a one-way ANOVA test. **(N)** Western blot against lysates of cells treated with indicated siRNAs and probed with NuMA, α-tubulin, and p37 antibodies. Bars, 10 µm.

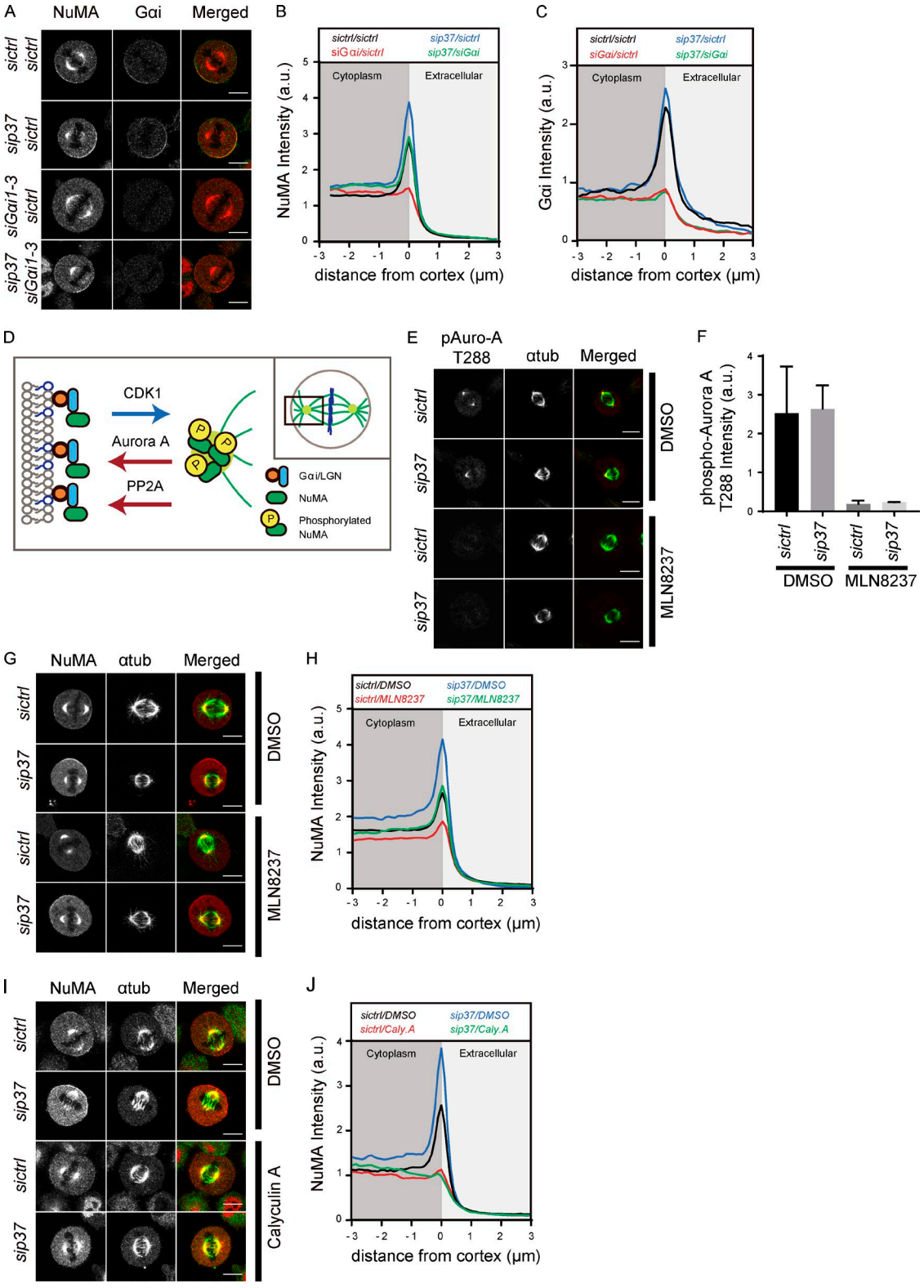

Figure 2. **High cortical NuMA levels in p37-depleted cells depend on a phosphatase but are independent of Gαi or Aurora A. (A–C)** Confocal images of HeLa cells stained for Gαi and NuMA (A) and corresponding cortical NuMA (B) and Gαi (C) line profiles in the indicated depletions. All line profiles represent the mean intensity across the cortex. *n* = 4–5; *n* = 72–112 cells. **(D)** Schematic representation of the regulation of NuMA localization by protein phosphorylation or dephosphorylation. **(E and F)** Confocal images of cells after indicated depletions and DMSO (0.01%) or MLN8237 (20 nM at 24 h) treatments stained for phospho-Aurora A (pT288) and α-tubulin (E) and corresponding quantification of centrosomal pT288–Aurora A (F). *n* = 2; *n* = 31–47. **(G and H)** The same cells as in E and F but stained for α-tubulin and NuMA (G) and corresponding cortical NuMA line profiles (H). *n* = 4; *n* = 80–97 cells. **(I and J)** Confocal images of cells stained for α-tubulin and NuMA after indicated depletions and DMSO (0.01%) or calyculin A (50 nM for 10 min) treatments (I) and corresponding cortical NuMA line profiles (J). *n* = 3; *n* = 59–65 cells. Error bars indicate SD. Bars, 10 μm.

p37 regulates NuMA levels via PP1

We next asked whether p37 regulates cortical NuMA levels via PP2A. As shown previously, PP2A depletion abolished cortical NuMA localization in *siControl* cells (Kotak et al., 2013); it did not, however, suppress the increase in cortical NuMA levels in *sip37* cells (Fig. 3, A–C). This suggests that PP2A is not the main phosphatase through which p37 regulates cortical NuMA levels. Calyculin A inhibits both PP2A and PP1 (Ishihara et al., 1989). Because exogenous p37 efficiently pulls down the PP1 isoform PP1α (Raman et al., 2015), we tested whether codepletion of the catalytic PP1α subunit impairs the excessive cortical recruitment of NuMA. PP1α depletion left cortical NuMA levels unchanged in control cells but abolished the excessive NuMA recruitment in *sip37* cells (Fig. 3, D–F) and restored normal spindle angles (median of 15.6° in *siControl/sip37*-treated cells versus 8.0° in *sipp1α/sip37* cells; Fig. 3 G). We conclude that p37 regulates cortical NuMA abundance via PP1.

Cdk1 and PP2A regulate NuMA in metaphase via threonine 2055 at the C terminus (Kotak et al., 2013; Seldin et al., 2013; Zheng et al., 2014). To test whether p37 regulates NuMA via the same site, we asked whether its depletion affects the localization of a phosphomimetic T2055E NuMA mutant. As previously shown, cortical GFP-NuMA-T2055E levels were reduced compared with GFP-NuMA in control depleted cells (Kotak et al., 2013), but in *sip37* cells, they were comparable, indicating that p37 regulates NuMA via a pathway that is separate from the one controlled by Cdk1 and PP2A (Fig. 3, H and I).

Our results infer that the excessive cortical NuMA levels observed in *sip37* cells are caused by high PP1 activity. PP1 activity could be generally higher in *sip37* cells, or p37 could spatially regulate PP1 activity. In metaphase, PP1α is enriched at kinetochores, where it stabilizes kinetochore–microtubule attachments and silences the spindle assembly checkpoint by dephosphorylating Aurora B kinase and its substrates (Murnion et al., 2001; Pinsky et al., 2009; Vanoosthuyse and Hardwick, 2009; Liu et al., 2010). When we compared PP1α levels at kinetochores in HeLa cells stably expressing GFP-PP1α, we found a significant reduction in *sip37* cells (Fig. 3, J and K). We also observed higher phospho–Aurora B (T232) levels on metaphase chromosomes, whereas Aurora B levels were unchanged (Fig. S2, A–D), consistent with lower PP1 activity. We conclude that p37 depletion does not lead to a generally higher PP1 activity in metaphase. We instead postulate that it leads to a lower PP1 activity at kinetochores and a higher cytoplasmic activity that promotes cortical NuMA localization.

PP1/Repo-Man controls cortical NuMA localization in metaphase

PP1 phosphatases are composed by a catalytic and a regulatory subunit. In human cells, there are ∼200 regulatory subunits each influencing PP1 localization, substrate specificity, and activity (Bollen et al., 2010). The two best-characterized mitotic regulatory PP1 subunits are Sds22 and Repo-Man (Trinkle-Mulcahy et al., 2006; Vagnarelli et al., 2006; Posch et al., 2010; Wurzenberger et al., 2012; Eiteneuer et al., 2014; Rodrigues et al., 2015). We codepleted either of them in *siControl* or *sip37* cells and measured cortical NuMA levels. Whereas Sds-22 depletion had no effect, depletion of Repo-Man abolished cortical NuMA enrichment both in *siControl* and *sip37* metaphase cells (Fig. 4, A–D; and Fig. S2, E and F), whereas it left Gαi and LGN levels unchanged (Fig. S2, G–J). This effect was not a result of an off-target effect, as a second validated Repo-Man siRNA also impaired cortical NuMA recruitment (Fig. S2 K; Wurzenberger et al., 2012). To validate that PP1/Repo-Man positively regulates NuMA localization at the cortex, we transiently overexpressed eGFP–Repo-Man or a mutant that cannot bind PP1, eGFP–Repo-Man^{RAXA} (Trinkle-Mulcahy et al., 2006), and monitored cortical NuMA levels and spindle orientation. eGFP–Repo-Man expression led to higher cortical NuMA levels than eGFP expression, whereas eGFP–Repo-Man^{RAXA} expression led to lower levels (Fig. 4, E and F). 63% of the cells expressing eGFP–Repo-Man but only 27% of the cells expressing eGFP–Repo-Man^{RAXA} and 13% of untransfected cells also showed excessive spindle rotations (Figs. 1 and 4, G and H). These excessive spindle rotations depended on NuMA because partial NuMA depletion suppressed this percentage to 29% in eGFP–Repo-Man–expressing cells (Fig. 4, I and J). We conclude that PP1/Repo-Man activity is essential for cortical recruitment of NuMA in metaphase and that p37 must restrain this activity to prevent spindle orientation defects caused by excessive cortical recruitment of NuMA.

p37 controls the PP1/Repo-Man–NuMA pathway specifically in metaphase

Cortical NuMA levels are temporally regulated as new Gαi-independent populations of NuMA are recruited to the cortex once cells enter anaphase (Kiyomitsu and Cheeseman, 2013; Seldin et al., 2013; Kotak et al., 2014). We thus investigated whether Repo-Man or p37 depletion also affect NuMA localization in anaphase (Fig. 5, A and B). Repo-Man depletion decreased cortical NuMA levels in anaphase. In contrast, *sip37* did not affect NuMA levels in anaphase. This indicates that PP1/Repo-Man activity positively regulates cortical NuMA in metaphase and anaphase and that p37 limits this activity specifically in metaphase.

Our results identify a novel regulatory pathway controlling the abundance of the NuMA–dynein motor complex at the cortex (Fig. 5 C): PP1/Repo-Man promote NuMA localization at the cortex but are kept in check by p37 until anaphase. A failure to do so leads to severe spindle orientation defects in metaphase as a result of excessive dynein-dependent forces. This argues that the PP1/Repo-Man complex has a more general role than just acting at kinetochores and/or chromatin, unlike what is currently thought. We further postulate that in anaphase, PP1 promotes recruitment of NuMA at the cortex in conjunction with PP2A. Future investigations will uncover how PP1/Repo-Man controls NuMA. NuMA has a PP1 binding motif (RVxF; Egloff et al., 1997), and mass spectroscopy analysis of PP1 immunoprecipitates identified NuMA (Moorhead et al., 2008), suggesting a direct interaction. In all our experiments, Repo-Man depletion had a stronger effect on NuMA than PP1α depletion, suggesting that Repo-Man might regulate NuMA in combination with several PP1 isoforms. A second important aspect of future investigation is the relationship between p37 and PP1/Repo-Man. Our data point to a local regulation as we find lower PP1 activity at kinetochores and higher NuMA levels at the cortex. We speculate that p37 mobilizes PP1/Repo-Man from cytoplasmic complexes in metaphase, allowing it to bind to kinetochores and chromatin. When p37 levels are low, high cytoplasmic PP1/Repo-Man activity dephosphorylates NuMA, which leads to higher cytoplasmic and cortical NuMA levels. This model is compatible with proteomic studies, which reported interactions between several PP1 subunits and p37 (Huttlin et al., 2015, 2017; Raman et al., 2015). Moreover, Shp1,

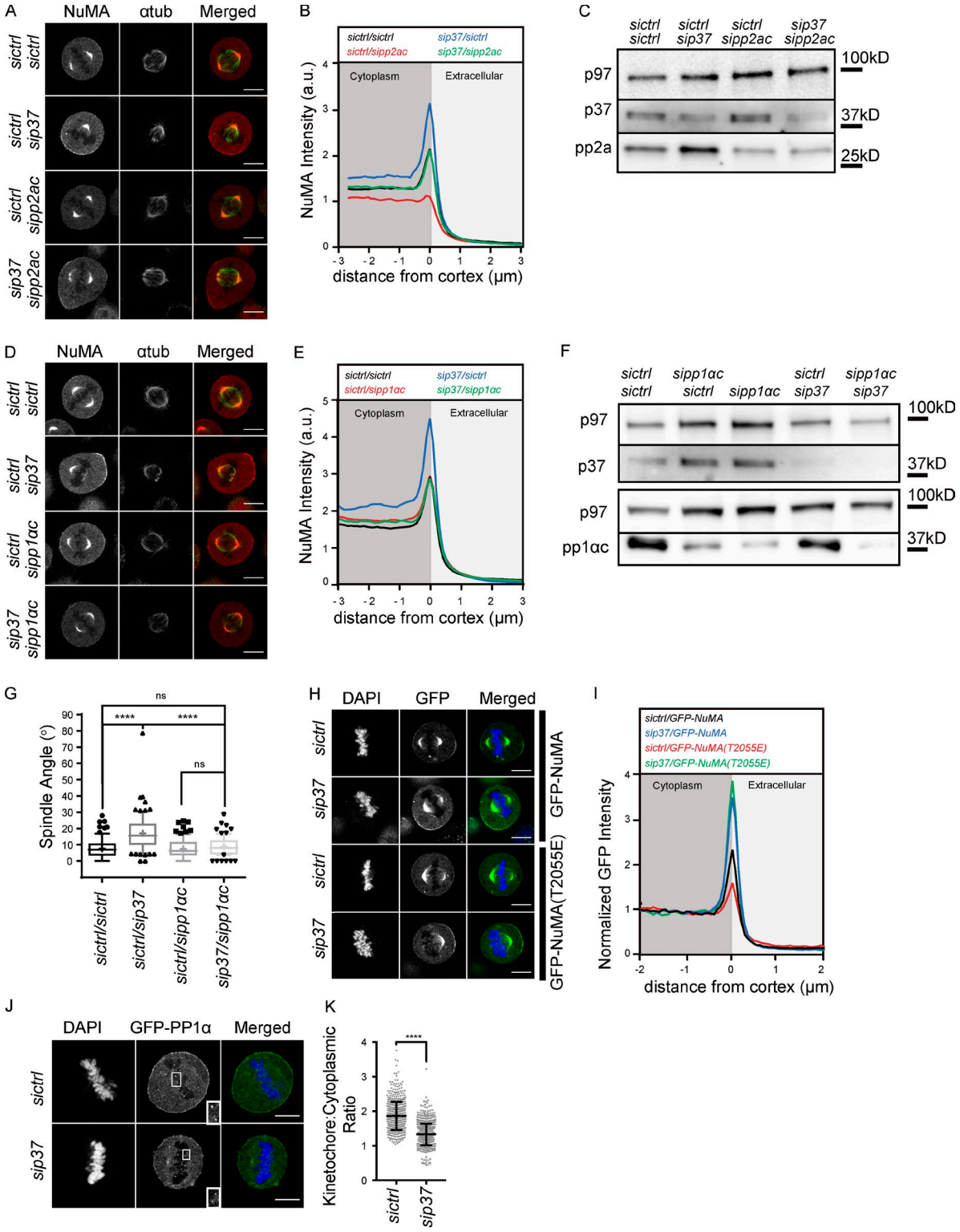

Figure 3. **p37 regulates cortical NuMA levels via PP1. (A and B)** Confocal images of HeLa cells stained for α-tubulin and NuMA after indicated depletions (A) and corresponding cortical NuMA line profiles (B). All line profiles represent the mean intensity across the cortex. *n* = 5; *n* = 109–112 cells. **(C)** Western blot of lysates of cells treated with indicated siRNAs and probed with p37, PP2a, and p97 (loading control) antibodies. **(D and E)** Confocal images of cells stained for α-tubulin and NuMA after indicated depletions (D) and corresponding cortical NuMA line profiles (E). *n* = 4; *n* = 102–104 cells. **(F)** Western blot of lysates of cells treated with indicated siRNAs and probed with p37, PP1ac, and p97 antibodies. The p37 and PP1ac immunoblots were run separately. **(G)** Quantification of spindle angles in cells treated with indicated siRNAs and stained with α-tubulin as in Fig. 1. *n* = 3; *n* = 73–85 cells. ****, P < 0.0001 in a Kruskal-Wallis test. **(H and I)** Confocal images of cells transfected with GFP-NuMA and GFP-NuMA (T2055E) stained with DAPI after indicated depletions (H) and corresponding normalized GFP-NuMA line profiles (I). *n* = 3; *n* = 45–56 cells. **(J and K)** Confocal images of *siControl* and *sip37* HeLa GFP-PP1α cells (J) and corresponding quantifications of GFP-PP1α levels at kinetochores (K). *n* = 3; *n* = 621–730. ****, P < 0.0001 in unpaired *t* tests. Bars, 10 µm.

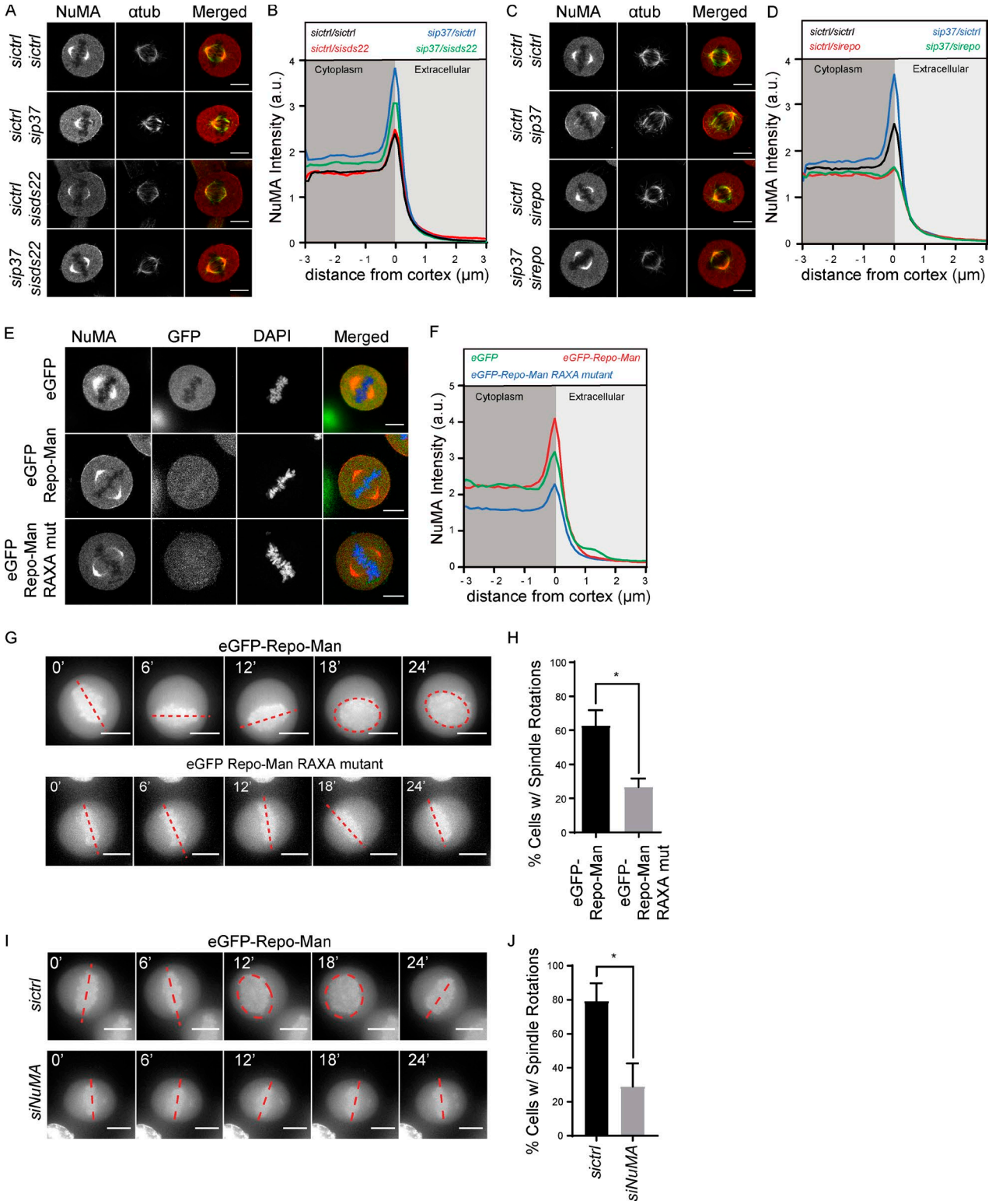

Figure 4. **PP1/Repo-Man controls cortical NuMA localization in metaphase. (A–D)** Confocal images of HeLa cells treated with indicated depletions and immunostained for NuMA and α-tubulin (A and C) and corresponding NuMA line profiles (B and D). All line profiles represent the mean intensity across the cortex. *n* = 3–4; *n* = 52–77 cells. **(E and F)** Confocal images of cells transiently expressing eGFP–Repo-Man, eGFP–Repo-Man^{RAXA}, or eGFP stained with NuMA antibodies and DAPI (DNA; E) and corresponding NuMA line profiles (F). *n* = 3; *n* = 49 cells. **(G)** Time-lapse images of metaphase HeLa cells transiently expressing eGFP–Repo-Man or eGFP–Repo-Man^{RAXA}. *t* = 0 min is set at the time of chromosome alignment. Red dashed lines indicate positions of metaphase plates, and dashed red circles indicate metaphase plates rotated by 90° in the z axis. **(H)** Mean percentage of transfected cells with spindle rotations. *n* = 4; *n* = 42–58 cells. *, P = 0.0128 in paired ratio *t* test. **(I)** Time-lapse images of metaphase cells transiently expressing eGFP–Repo-Man treated with control or NuMA siRNA and labeled as in G. **(J)** Mean percentages of transfected cells with spindle rotations. *n* = 5; *n* = 32–34 cells. *, P = 0.0140 in a paired ratio *t* test. Error bars indicate SEM. Bars, 10 μm.

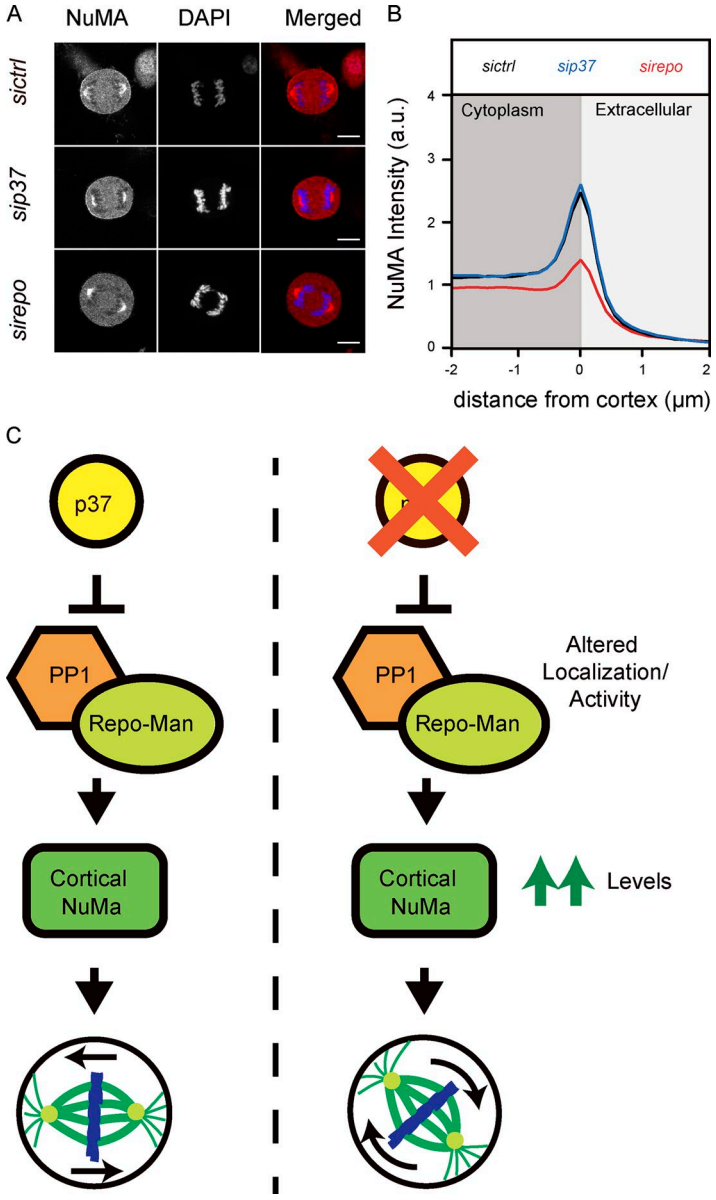

Figure 5. **p37 controls the PP1/Repo-Man–NuMA pathway specifically in metaphase. (A)** Confocal images of anaphase HeLa cells treated with indicated siRNAs and stained with NuMA antibodies and DAPI (DNA). Bars, 10 µm. **(B)** The corresponding NuMA line profile represents the mean intensity across the cortex. *n* = 3; *n* = 76–80 cells. **(C)** Working model: p37 negatively regulates PP1/Repo-Man to limit cortical NuMA in metaphase.

the *Saccharomyces cerevisiae* orthologue of p37, positively regulates nuclear accumulation of yeast PP1 (called Glc7) to promote Glc7 activity at kinetochores (Cheng and Chen, 2010; Böhm and Buchberger, 2013), suggesting that the overall principle of the pathway is conserved.

Materials and methods

Cell culture methods and drug treatments

HeLa Kyoto cells and HeLa dynein heavy chain–GFP cells (gift from I. Cheeseman, Massachusetts Institute of Technology, Cambridge, MA) were grown in DMEM containing 10% FCS, 100 U/ml penicillin, and 100 mg/ml streptomycin at 37°C with 5% CO_2 in a humidified incubator. HeLa eGFP-centrin1/eGFP–CENP-A cells were supplemented with 0.2 mg/ml of G418 and 0.5 µg/ml of puromycin. HeLa GFP-PP1α cells (GA4.3; gift from L. Trinkle-Mulcahy; Trinkle-Mulcahy et al., 2006) were supplemented with 0.4 mg/ml of G418. Live-cell imaging experiments were performed at 37°C in Lab-TekII (Thermo Fisher Scientific) and Ibidi chambers in Leibovitz's medium (L15) supplemented with 10% FCS. For drug treatments, Aurora A was inhibited for 24 h with 20 nM MLN8237 (Selleckchem) and PP1/PP2A for 10 min with 50 µM calyculin A (Thermo Fisher Scientific; Ishihara et al., 1989). To visualize microtubules during live-cell imaging, 50 nM SiR-tubulin (Spirochrome AG) was added to the cells 3 h before acquisition. To synchronize HeLa cells in mitosis, cells were treated for 14 h with 20 µM of the Eg5 inhibitor (+)-*S*-Trityl-L-cysteine (Sigma-Aldrich).

siRNA and plasmid transfections

The siRNA oligonucleotides used for protein depletions (Thermo Fisher Scientific, GE Healthcare, or QIAGEN) were all already validated by other laboratories (references cited for each siRNA) and are as follows: control (scrambled, 5′-GGACCUGGAGGUCUG CUGU-3′; Mchedlishvili et al., 2012), p37 (5′-CUCCAGAAGAGG AGGAUAA-3′; Uchiyama et al., 2006), NuMA (5′-GGCGUGGCA GGAGAG-3′; Kiyomitsu and Cheeseman, 2013), $G\alpha i_{1/3}$ (5′-CCGAAU GCAUGAAAGCAUG-3′; Kiyomitsu and Cheeseman, 2013), $G\alpha i_2$ (5′-CUUGAGCGCCUAUGACUUG-3′; Kiyomitsu and Cheeseman, 2013), LGN (SMARTpool, 5′-GAACUAACAGCACGACUUA-3′, 5′-CUUCAGGGAUGCAGUUAUA-3′, 5′-ACAGUGAAAUUCUUG

CUAA-3′, and 5′-UGAAGGGUUCUUUGACUUA-3′; Kiyomitsu and Cheeseman, 2012), PP1αc (5′-CCGCAATTCCGCCAAAGCCAA-3′; Wurzenberger et al., 2012), PP2Ac (5′-ATGGAACTTGACGATACT CTA-3′; Kotak et al., 2013), Repo-Man (5′-ATGGGACTCATCCGA GCTTAA-3′ in all figures except Fig. S2 and 5′-AGCAAATACTCC ATTGCGTAA-3′ in Fig. S2; Wurzenberger et al., 2012), and Sds22 (5′-AGAGTTCTGGATGAACGACAA-3′; Wurzenberger et al., 2012). Cells were transfected with siRNAs for 48 h unless otherwise indicated at final concentrations of 50 nM using Lipofectamine RNAiMAX (Thermo Fisher Scientific). For codepletion experiments, selected siRNA oligonucleotides were transfected at a 1:1 ratio with a total concentration of 50 nM. For gene expression, the following plasmids were used: pEGFP-C1 (Invitrogen), pEGFP-(C1)–Repo-Man, and pEGFP-(C1)–Repo-Man/RAXA (gift from A. Lamond; plasmids 44212 and 44213; Addgene Trinkle-Mulcahy et al., 2006), GFP-NuMA-FL, and GFP-NuMA-T2055E (gift from P. Gönzcy; Kotak et al., 2013). Cells were transfected with 0.5–2 µg of plasmid DNA using Lipofectamine 2000 (Invitrogen) and analyzed 24 h after transfection. For experiments involving siRNA and plasmid DNA transfection, the siRNA and DNA were added to the cells 48 and 24 h before analysis, respectively.

Immunofluorescence

Cells were fixed with 4% formaldehyde/0.2% glutaraldehyde (in PBS) for 15 min at room temperature. Slides were washed for 5 min with PBS/NH_4Cl (50 mM), washed twice with PBS, and incubated overnight with primary antibodies diluted in permeabilization buffer (20 mM Pipes, 0.5% saponin, 5% BSA, 137 mM NaCl, and 2.7 mM KCl, pH 6.8) at 4°C in a wet chamber. The slides were washed, incubated at room temperature with secondary antibodies diluted in permeabilization buffer for 45 min, and mounted on Vectashield with DAPI (Vector Laboratories). For immunofluorescence of HeLa GFP-PP1α (GA4.3), cells were fixed with 4% formaldehyde and 0.1% Triton X-100, and then slides were washed with PBS and mounted on Vectashield with DAPI. Alternatively, cells were fixed with methanol at −20°C for 4 min, washed with PBS, blocked for 1 h with 1% PBS/BSA, and incubated overnight with primary antibodies (in PBS/1% BSA) at 4°C in a wet chamber. After PBS washes, slides were incubated with secondary antibodies (in PBS/1% BSA) for 45 min at room temperature, washed with PBS, and mounted on Vectashield with DAPI. The following primary antibodies were used: anti-NuMA (rabbit; 1:500; Abcam), anti-Gαi (mouse; 1:200; Santa Cruz Biotechnology, Inc.), anti-$p150^{glued}$ (mouse; 1:400; BD), anti–Aurora B (rabbit; 1:1,000; McClelland et al., 2007), antiphospho–Aurora B T232 (rabbit; 1:1,000; Rockland Inc.), antiphospho–Aurora A T288 (rabbit; 1:1,500; Cell Signaling Technology), anti–α-tubulin (mouse; 1:1,000; Sigma-Aldrich), anti–γ-tubulin (rabbit; 1:1,000; Sigma-Aldrich), anti-MPM2 (mitotic proteins; mouse; 1:1,000; Abcam), and anti-LGN (rabbit; 1:400; Sigma-Aldrich). For secondary antibodies, cross-adsorbed Alexa Fluor–conjugated antibodies (1:400; Invitrogen) were used.

Image acquisition, live-cell imaging, and image quantification

Images for immunofluorescence were acquired using either an A1r spectral confocal microscope (Nikon) or an LSM800 Airyscan confocal microscope (ZEISS). The A1r spectral (inverted T*i* Eclipse) confocal microscope is equipped with four PMTs, including two highly sensitive detectors (GaAsP) for green and red channels. Experiments were performed with a 60× 1.4 NA CFI Plan Apochromat Lambda oil objective, and NIS Elements AR software (v.4.20.01; Nikon) was used to set acquisition parameters. The LSM800 Airyscan confocal microscope was equipped with two high-sensitive GaAsP photomultiplier tube detectors. Experiments were performed with a Plan Apochromat 63× 1.40 NA oil objective, and ZEN software (v.2.3; ZEISS) was used to set acquisition parameters. Live-cell imaging was performed for 8–12 h at 37°C on the T*i* widefield microscope (Nikon) equipped with an environmental chamber using a 60× 1.3 NA oil objective and a CoolSNAP HQ camera (Roper Scientific) at a sampling rate of 3 min, recording at each time point of 12 z stacks separated by 1 µm using NIS Elements AR software. The recorded images were quantified using FIJI software (ImageJ; National Institutes of Health) and Imaris (7.7.1; Bitplane). TIFF or PNG images were mounted into figures using CS Photoshop and CS Illustrator (Adobe).

The spindle rotation phenotype was scored in time-lapse videos by analyzing mean changes in angle/position of the metaphase spindle over time through live-cell imaging. To determine the spindle angle in fixed metaphase cells, cells were stained for γ- or α-tubulin. The x, y, and z coordinates of the spindle poles were obtained, and the spindle angle was calculated by applying the spindle pole coordinates to the trigonometric function shown in Fig. S3 A. The levels of cortical protein were measured by overlaying a 3-pixel-wide line on the cortex of a metaphase cell to obtain the mean intensity (Fig. S3 B). To quantify chromosomal Aurora B and phosphor–T232 Aurora B in metaphase, the DAPI image was used to build a mask for measuring the mean intensity value of the fluorescence signal on chromatin, and the same mask was used to correct for background (Fig. S3 C). To obtain the line profile of cortical proteins, a 10-pixel-wide × 6-µm-long line scan overlapping the cortex was used (Fig. S3 D). The line profiles of individual cells were first averaged within an experiment before calculating the mean between experiments. To quantify cortical NuMA levels around the entire cortex, we generated an intensity profile in metaphase using ImageJ (Fig. S3 E). To obtain the volume of NuMA at spindle poles, we applied a threshold function to the immunofluorescence images and performed the measurement using Imaris software (Fig. S3 F). To quantify GFP-PP1α at kinetochores, we determined the ratio between GFP signal intensities at kinetochores and normalized it with the cytoplasmic GFP signal (Fig. S3 G).

Western blotting

For cell extracts, cells were harvested in lysis buffer (150 mM KCl, 50 mM Tris, pH 7.4, 5 mM $MgCl_2$, 5% glycerol, 1% Triton X-100, 2 mM β-mercaptoethanol supplemented with EDTA-free protease inhibitor, and PhosSTOP phosphatase inhibitor [Roche]) and incubated on ice for 1 h. After centrifugation for 20 min at 13,000 rpm, the protein concentration in the supernatant was determined in a Bradford assay (Bio-Rad Laboratories) using a UV/Vis Spectrophotomer (MicroDigital). Alternatively, to quantify total NuMA levels, cells were directly harvested in Laemmli sample buffer and boiled for 10 min before mechanical shearing through a 26G syringe tip. The following primary antibodies were used: anti-NuMA (rabbit; 1:1,000; Abcam), anti-PP2Ac (rabbit; 1:1,000; EMD Millipore), anti-PP1αc (rabbit; 1:1,000; Cell Signaling Technology), anti-p97 (rabbit; 1:1.000; a gift from H. Meyer; Cao et al., 2003), anti-p37 (rabbit; 1.15 µg/µl; this study), and anti–Repo-Man (rabbit; 1:2,000; Cell Signaling Technology). The following HRP-conjugated secondary antibodies were used: ECL anti–rabbit IgG (GE Healthcare) and anti–mouse IgG (Bio-Rad Laboratories). Proteins were separated by SDS-PAGE and transferred onto nitrocellulose membranes by wet blotting. Protein bands were detected using the ECL Prime Western Blotting Detection reagent (GE Healthcare) and a PXi/PXi Touch luminescence detector (Syngene). Protein bands were quantified with ImageJ as described in the method outlined at http://lukemiller.org/index.php/2010/11/-analyzing-gels-and-western-blots-with-image-j/.

Antibody production

The full-length p37 cDNA was subcloned by Gateway technology (Invitrogen) into the pDEST–maltose-binding protein (MBP) vector. Recombinant MBP-tagged p37 (MBP-p37) protein expression was induced in BL21 *Escherichia coli* and purified using standard column purification on an amylose resin (New England Biolabs, Inc.) column. Purified MBP-p37 was used to immunize two rabbits with a standard immunization protocol (Moravian-Biotechnology). The anti-p37 serum was affinity purified on membrane strips carrying bacterially expressed GST-p37 antigen.

Statistical methods

Outliers in fluorescent intensity quantifications were determined and removed from data using the modified Thompson Tau method. Paired two-tailed *t* tests, one-way ANOVA tests, Mann-Whitney tests, and Kruskal-Wallis tests were run on PRISM (7.02; GraphPad Software). Graphs were plotted in PRISM and mounted in Illustrator. Box blots show median, lower, and upper quartiles (line and box), 10th and 90th percentiles (whiskers), and means (+).

Online supplemental material

Fig. S1 is related to Figs. 1 and 2 and shows quantification of spindle angle in p37-depleted cells, characterization of spindle rotation, characterization of the p37 antibody, cortical LGN and NuMA levels in LGN and LGN/p37 depletions, MPM2 data, and levels of Gαi and LGN in control and calyculin A–treated cells. Fig. S2 is related to Figs. 3 and 4 and shows chromosomal Aurora B and phospho–T232 Aurora B levels in p37-depleted cells, Western blotting of the lysates of controls and the codepletion of Sds-22 and Repo-Man with p37, corresponding quantifications and Gαi and LGN staining in the Repo-Man and Repo-Man/p37 depletions, and NuMA line profile after depletion of Repo-Man with a second independent siRNA. Fig. S3 is related to the Image acquisition, live-cell imaging, and image quantification section of the Materials and methods and illustrates how the data presented in the manuscript were quantified.

Acknowledgments

Authors are grateful to P. Gönczy (Swiss Federal Institute of Technology in Lausanne, Lausanne, Switzerland), Q. Du (Augusta University, Augusta, Georgia), L. Trinkle-Mulcahy (University of Ottawa, Ottawa, Canada), I. Cheeseman, H. Meyer (University of Essen, Essen, Germany), and the MitoCheck consortium for reagents and cell lines, the Bioimaging platform of the Medical Faculty of the University of Geneva for microscopy support, and M. Bollen (University of Leuven, Leuven, Belgium), H. Meyer, and the members of the Gotta and Meraldi laboratories for helpful discussions, and Daniela Harry for technical support.

Work in the Gotta laboratory is supported by a Swiss National Science Foundation project grant (31003A_156013) and the University of Geneva, and in the Meraldi laboratory by a Swiss National Science Foundation project grant (31003A_160006) and the University of Geneva.

The authors declare no competing financial interests.

Author contributions: the project was initiated and directed by P. Meraldi and M. Gotta. All experiments were carried out by B.H. Lee with help from F. Schwager. B.H. Lee, P. Meraldi, and M. Gotta interpreted the data and wrote the manuscript.

Submitted: 12 July 2017
Revised: 27 October 2017
Accepted: 16 November 2017

References

Bird, S.L., R. Heald, and K. Weis. 2013. RanGTP and CLASP1 cooperate to position the mitotic spindle. *Mol. Biol. Cell.* 24:2506–2514. https://doi.org/10.1091/mbc.E13-03-0150

Böhm, S., and A. Buchberger. 2013. The budding yeast Cdc48(Shp1) complex promotes cell cycle progression by positive regulation of protein phosphatase 1 (Glc7). *PLoS One.* 8:e56486. https://doi.org/10.1371/journal.pone.0056486

Bollen, M., W. Peti, M.J. Ragusa, and M. Beullens. 2010. The extended PP1 toolkit: designed to create specificity. *Trends Biochem. Sci.* 35:450–458. https://doi.org/10.1016/j.tibs.2010.03.002

Cao, K., R. Nakajima, H.H. Meyer, and Y. Zheng. 2003. The AAA-ATPase Cdc48/p97 regulates spindle disassembly at the end of mitosis. *Cell.* 115:355–367. https://doi.org/10.1016/S0092-8674(03)00815-8

Cheng, Y.L., and R.H. Chen. 2010. The AAA-ATPase Cdc48 and cofactor Shp1 promote chromosome bi-orientation by balancing Aurora B activity. *J. Cell Sci.* 123:2025–2034. https://doi.org/10.1242/jcs.066043

di Pietro, F., A. Echard, and X. Morin. 2016. Regulation of mitotic spindle orientation: an integrated view. *EMBO Rep.* 17:1106–1130. https://doi.org/10.15252/embr.201642292

Du, Q., and I.G. Macara. 2004. Mammalian Pins is a conformational switch that links NuMA to heterotrimeric G proteins. *Cell.* 119:503–516. https://doi.org/10.1016/j.cell.2004.10.028

Egloff, M.P., D.F. Johnson, G. Moorhead, P.T.W. Cohen, P. Cohen, and D. Barford. 1997. Structural basis for the recognition of regulatory subunits by the catalytic subunit of protein phosphatase 1. *EMBO J.* 16:1876–1887. https://doi.org/10.1093/emboj/16.8.1876

Eiteneuer, A., J. Seiler, M. Weith, M. Beullens, B. Lesage, V. Krenn, A. Musacchio, M. Bollen, and H. Meyer. 2014. Inhibitor-3 ensures bipolar mitotic spindle attachment by limiting association of SDS22 with kinetochore-bound protein phosphatase-1. *EMBO J.* 33:2704–2720. https://doi.org/10.15252/embj.201489054

Gallini, S., M. Carminati, F. De Mattia, L. Pirovano, E. Martini, A. Oldani, I.A. Asteriti, G. Guarguaglini, and M. Mapelli. 2016. NuMA Phosphorylation by Aurora-A Orchestrates Spindle Orientation. *Curr. Biol.* 26:458–469. https://doi.org/10.1016/j.cub.2015.12.051

Gordon, M.B., L. Howard, and D.A. Compton. 2001. Chromosome movement in mitosis requires microtubule anchorage at spindle poles. *J. Cell Biol.* 152:425–434. https://doi.org/10.1083/jcb.152.3.425

Huttlin, E.L., L. Ting, R.J. Bruckner, F. Gebreab, M.P. Gygi, J. Szpyt, S. Tam, G. Zarraga, G. Colby, K. Baltier, et al. 2015. The BioPlex Network: A Systematic Exploration of the Human Interactome. *Cell.* 162:425–440. https://doi.org/10.1016/j.cell.2015.06.043

Huttlin, E.L., R.J. Bruckner, J.A. Paulo, J.R. Cannon, L. Ting, K. Baltier, G. Colby, F. Gebreab, M.P. Gygi, H. Parzen, et al. 2017. Architecture of the human interactome defines protein communities and disease networks. *Nature.* 545:505–509. https://doi.org/10.1038/nature22366

Ishihara, H., B.L. Martin, D.L. Brautigan, H. Karaki, H. Ozaki, Y. Kato, N. Fusetani, S. Watabe, K. Hashimoto, D. Uemura, and D.J. Hartshome. 1989. Calyculin A and okadaic acid: inhibitors of protein phosphatase activity. *Biochem. Biophys. Res. Commun.* 159:871–877. https://doi.org/10.1016/0006-291X(89)92189-X

Kiyomitsu, T., and I.M. Cheeseman. 2012. Chromosome- and spindle-pole-derived signals generate an intrinsic code for spindle position and orientation. *Nat. Cell Biol.* 14:311–317. https://doi.org/10.1038/ncb2440

Kiyomitsu, T., and I.M. Cheeseman. 2013. Cortical dynein and asymmetric membrane elongation coordinately position the spindle in anaphase. *Cell.* 154:391–402. https://doi.org/10.1016/j.cell.2013.06.010

Kotak, S., C. Busso, and P. Gönczy. 2012. Cortical dynein is critical for proper spindle positioning in human cells. *J. Cell Biol.* 199:97–110. https://doi.org/10.1083/jcb.201203166

Kotak, S., C. Busso, and P. Gönczy. 2013. NuMA phosphorylation by CDK1 couples mitotic progression with cortical dynein function. *EMBO J.* 32:2517–2529. https://doi.org/10.1038/emboj.2013.172

Kotak, S., C. Busso, and P. Gönczy. 2014. NuMA interacts with phosphoinositides and links the mitotic spindle with the plasma membrane. *EMBO J.* 33:1815–1830. https://doi.org/10.15252/embj.201488147

Kotak, S., K. Afshar, C. Busso, and P. Gönczy. 2016. Aurora A kinase regulates proper spindle positioning in C. elegans and in human cells. *J. Cell Sci.* 129:3015–3025. https://doi.org/10.1242/jcs.184416

Kress, E., F. Schwager, R. Holtackers, J. Seiler, F. Prodon, E. Zanin, A. Eiteneuer, M. Toya, A. Sugimoto, H. Meyer, et al. 2013. The UBXN-2/p37/p47 adaptors of CDC-48/p97 regulate mitosis by limiting the centrosomal recruitment of Aurora A. *J. Cell Biol.* 201:559–575. https://doi.org/10.1083/jcb.201209107

Liu, D., M. Vleugel, C.B. Backer, T. Hori, T. Fukagawa, I.M. Cheeseman, and M.A. Lampson. 2010. Regulated targeting of protein phosphatase 1 to

the outer kinetochore by KNL1 opposes Aurora B kinase. *J. Cell Biol.* 188:809–820. https://doi.org/10.1083/jcb.201001006

Lukinavičius, G., L. Reymond, E. D'Este, A. Masharina, F. Göttfert, H. Ta, A. Güther, M. Fournier, S. Rizzo, H. Waldmann, et al. 2014. Fluorogenic probes for live-cell imaging of the cytoskeleton. *Nat. Methods.* 11:731–733. https://doi.org/10.1038/nmeth.2972

McClelland, S.E., S. Borusu, A.C. Amaro, J.R. Winter, M. Belwal, A.D. McAinsh, and P. Meraldi. 2007. The CENP-A NAC/CAD kinetochore complex controls chromosome congression and spindle bipolarity. *EMBO J.* 26:5033–5047. https://doi.org/10.1038/sj.emboj.7601927

Mchedlishvili, N., S. Wieser, R. Holtackers, J. Mouysset, M. Belwal, A.C. Amaro, and P. Meraldi. 2012. Kinetochores accelerate centrosome separation to ensure faithful chromosome segregation. *J. Cell Sci.* 125:906–918. https://doi.org/10.1242/jcs.091967

Merdes, A., K. Ramyar, J.D. Vechio, and D.W. Cleveland. 1996. A complex of NuMA and cytoplasmic dynein is essential for mitotic spindle assembly. *Cell.* 87:447–458. https://doi.org/10.1016/S0092-8674(00)81365-3

Moorhead, G.B., L. Trinkle-Mulcahy, M. Nimick, V. De Wever, D.G. Campbell, R. Gourlay, Y.W. Lam, and A.I. Lamond. 2008. Displacement affinity chromatography of protein phosphatase one (PP1) complexes. *BMC Biochem.* 9:28. https://doi.org/10.1186/1471-2091-9-28

Murnion, M.E., R.R. Adams, D.M. Callister, C.D. Allis, W.C. Earnshaw, and J.R. Swedlow. 2001. Chromatin-associated protein phosphatase 1 regulates aurora-B and histone H3 phosphorylation. *J. Biol. Chem.* 276:26656–26665. https://doi.org/10.1074/jbc.M102288200

Panousopoulou, E., and J.B. Green. 2014. Spindle orientation processes in epithelial growth and organisation. *Semin. Cell Dev. Biol.* 34:124–132. https://doi.org/10.1016/j.semcdb.2014.06.013

Pinsky, B.A., C.R. Nelson, and S. Biggins. 2009. Protein phosphatase 1 regulates exit from the spindle checkpoint in budding yeast. *Curr. Biol.* 19:1182–1187. https://doi.org/10.1016/j.cub.2009.06.043

Posch, M., G.A. Khoudoli, S. Swift, E.M. King, J.G. Deluca, and J.R. Swedlow. 2010. Sds22 regulates aurora B activity and microtubule-kinetochore interactions at mitosis. *J. Cell Biol.* 191:61–74. https://doi.org/10.1083/jcb.200912046

Raman, M., M. Sergeev, M. Garnaas, J.R. Lydeard, E.L. Huttlin, W. Goessling, J.V. Shah, and J.W. Harper. 2015. Systematic proteomics of the VCP-UBXD adaptor network identifies a role for UBXN10 in regulating ciliogenesis. *Nat. Cell Biol.* 17:1356–1369. https://doi.org/10.1038/ncb3238

Rodrigues, N.T., S. Lekomtsev, S. Jananji, J. Kriston-Vizi, G.R. Hickson, and B. Baum. 2015. Kinetochore-localized PP1-Sds22 couples chromosome segregation to polar relaxation. *Nature.* 524:489–492. https://doi.org/10.1038/nature14496

Seldin, L., N.D. Poulson, H.P. Foote, and T. Lechler. 2013. NuMA localization, stability, and function in spindle orientation involve 4.1 and Cdk1 interactions. *Mol. Biol. Cell.* 24:3651–3662. https://doi.org/10.1091/mbc.E13-05-0277

Tame, M.A., J.A. Raaijmakers, P. Afanasyev, and R.H. Medema. 2016. Chromosome misalignments induce spindle-positioning defects. *EMBO Rep.* 17:317–325. https://doi.org/10.15252/embr.201541143

Toyoshima, F., and E. Nishida. 2007. Integrin-mediated adhesion orients the spindle parallel to the substratum in an EB1- and myosin X-dependent manner. *EMBO J.* 26:1487–1498. https://doi.org/10.1038/sj.emboj.7601599

Trinkle-Mulcahy, L., J. Andersen, Y.W. Lam, G. Moorhead, M. Mann, and A.I. Lamond. 2006. Repo-Man recruits PP1 gamma to chromatin and is essential for cell viability. *J. Cell Biol.* 172:679–692. https://doi.org/10.1083/jcb.200508154

Uchiyama, K., G. Totsukawa, M. Puhka, Y. Kaneko, E. Jokitalo, I. Dreveny, F. Beuron, X. Zhang, P. Freemont, and H. Kondo. 2006. p37 is a p97 adaptor required for Golgi and ER biogenesis in interphase and at the end of mitosis. *Dev. Cell.* 11:803–816. https://doi.org/10.1016/j.devcel.2006.10.016

Vagnarelli, P., D.F. Hudson, S.A. Ribeiro, L. Trinkle-Mulcahy, J.M. Spence, F. Lai, C.J. Farr, A.I. Lamond, and W.C. Earnshaw. 2006. Condensin and Repo-Man-PP1 co-operate in the regulation of chromosome architecture during mitosis. *Nat. Cell Biol.* 8:1133–1142. https://doi.org/10.1038/ncb1475

Vanoosthuyse, V., and K.G. Hardwick. 2009. A novel protein phosphatase 1-dependent spindle checkpoint silencing mechanism. *Curr. Biol.* 19:1176–1181. https://doi.org/10.1016/j.cub.2009.05.060

Westendorf, J.M., P.N. Rao, and L. Gerace. 1994. Cloning of cDNAs for M-phase phosphoproteins recognized by the MPM2 monoclonal antibody and determination of the phosphorylated epitope. *Proc. Natl. Acad. Sci. USA.* 91:714–718. https://doi.org/10.1073/pnas.91.2.714

Woodard, G.E., N.N. Huang, H. Cho, T. Miki, G.G. Tall, and J.H. Kehrl. 2010. Ric-8A and Gi alpha recruit LGN, NuMA, and dynein to the cell cortex to help orient the mitotic spindle. *Mol. Cell. Biol.* 30:3519–3530. https://doi.org/10.1128/MCB.00394-10

Wurzenberger, C., M. Held, M.A. Lampson, I. Poser, A.A. Hyman, and D.W. Gerlich. 2012. Sds22 and Repo-Man stabilize chromosome segregation by counteracting Aurora B on anaphase kinetochores. *J. Cell Biol.* 198:173–183. https://doi.org/10.1083/jcb.201112112

Yamanaka, K., Y. Sasagawa, and T. Ogura. 2012. Recent advances in p97/VCP/Cdc48 cellular functions. *Biochim. Biophys. Acta.* 1823:130–137. https://doi.org/10.1016/j.bbamcr.2011.07.001

Zheng, Z., Q. Wan, G. Meixiong, and Q. Du. 2014. Cell cycle-regulated membrane binding of NuMA contributes to efficient anaphase chromosome separation. *Mol. Biol. Cell.* 25:606–619. https://doi.org/10.1091/mbc.E13-08-0474